Science Advances
AAAS

advances.sciencemag.org/cgi/content/full/5/1/eaat2953/DC1

Supplementary Materials for

A self-illuminating nanoparticle for inflammation imaging and cancer therapy

Xiaoqiu Xu, Huijie An, Dinglin Zhang, Hui Tao, Yin Dou, Xiaohui Li, Jun Huang, Jianxiang Zhang*

*Corresponding author. Email: jxzhang@tmmu.edu.cn

Published 9 January 2019, *Sci. Adv.* **5**, eaat2953 (2019)
DOI: 10.1126/sciadv.aat2953

This PDF file includes:

Supplementary Materials and Methods

Materials

5-Amino-2,3-dihydrophthalazine-1,4-dione (luminol), 4-aminobenzoic hydrazide (4-ABAH), 4-hydroxy-2,2,6,6-tetramethylpiperidine 1-oxyl (Tempol), 1-ethyl-3-(3-dimethylaminopropyl)carbodiimide hydrochloride (EDC), N-hydroxysuccinimide (NHS), 2',7'-dichlorofluorescin diacetate (DCF-DA), phorbol 12-myristate 13-acetate (PMA), zymosan, thiazolylblue tetrazolium bromide (MTT), anti-β-actin antibody, acetaminophen (APAP), 4',6-diamidino-2-phenylindole (DAPI), and in situ cell death detection kit of terminal deoxynucleotidyl transferase dUTP nick end labeling (TUNEL) were purchased from Sigma-Aldrich (St. Louis, U.S.A.). Monomethyl terminated polyethylene glycol monoamine (PEG-NH_2) with M_w of 2, 000 was purchased from Laysan Bio, Inc. Chlorin e6 (Ce6) was purchased from Frontier Scientific (UT, U.S.A.). Myeloperoxidase (MPO) was obtained from BioVision Inc. LysoTracker Green DND-26 (Lyso), MitoTracker Green FM (Mitotracker), and Amplex red hydrogen peroxide/peroxidase assay kit were obtained from Invitrogen (U.S.A.). Antibodies to caspase-3 (#9662, dilution 1:1,000), cleaved caspase-3 (#9664, dilution 1:1,000), caspase-8 (#9746, dilution 1:1,000), and caspase-9 (#9508, dilution 1:1,000) were purchased from Cell Signaling Technology (Boston, U.S.A.). Anti-PCNA rabbit polyclonal antibody was purchased from Servicebio (Wuhan, China). Tetramethylrhodamine ethyl ester (TMRE) mitochondrial membrane potential assay kit was purchased from Abcam (Cambridge, UK). FITC Annexin V apoptosis detection kit with propidium iodide (PI), anti-mouse Ly-6G antibody, and anti-CD11b antibody were from Biolegend (San Diego, CA, U.S.A.). Mouse MPO antibody was obtained from R&D Systems Inc. (Minneapolis, U.S.A.). Dulbecco's modified Eagle's medium (DMEM) medium, RPMI-1640 medium, trypsin, penicillin, streptomycin, and fetal bovine serum (FBS) were purchased from HyClone (Waltham, U.S.A). Diphenylanthracene (DPA) was purchased from Aladdin (Shanghai, China). Dextran sodium sulfate (DSS) with M_w of 35 kDa was obtained from MP Biomedical (U.S.A.). Cisplatin injection (CDDP) was supplied by Qilu Pharmaceutical Co., Ltd (Jinan, China). All the other reagents are commercially available and used as received.

Materials characterization

^{1}H NMR spectra were acquired on a 600 MHz spectrometer (DD2, Agilent). Mass spectroscopy was analyzed by electrospray ionization mass spectrometry (ESI-MS) with a SQ detector (Waters, U.S.A.). Matrix-assisted laser desorption/ionization time-of-flight (MALDI-TOF) mass spectrometry was performed on a MALDI-7090 TOF-TOF mass spectrometer (Shimadzu). Fourier-transform infrared (FT-IR) spectra were recorded on a PerkinElmer FT-IR spectrometer (100S, U.S.A.). UV-visible absorbance curves were recorded on a TU-1901 spectrometer (Beijing Purkinje General Instrument, China). Fluorescence spectroscopy analyses were carried out on a F-7000 spectrometer (Hitachi, Japan).

Preparation and characterization of CLP nanoparticles

CLP nanoparticles were obtained by directly dissolved CLP conjugate in aqueous solution at defined concentrations. Particle size, size distribution profiles, and ζ-potential values of CLP nanoparticles were detected with a Malvern Zetasizer Nano ZS instrument at 25°C. Unless otherwise stated, deionized water was used as the solvent for CLP nanoparticles. Transmission electron microscopy (TEM) observation was performed using a JEM-1400 microscope (JEOL, Japan).

Cell culture

RAW264.7 murine macrophage, MOVAS mouse aortic vascular smooth muscle cell, mouse melanoma cell B16F10, human breast cancer cell MCF-7, and A549 human lung carcinoma cell were purchased from the Cell Bank of the Committee on Type Culture Collection of Chinese Academy of Sciences (Shanghai, China). Cells were cultured in growth medium containing 10% FBS, 100 U/ml of penicillin, and 100 mg/ml of streptomycin at 37°C in a humidified atmosphere of 5% CO_2. A549 and RAW264.7 cells were cultured in RPMI 1640 medium, while B16F10, MCF-7 and MOVAS were cultured in DMEM medium.

Quantification of inflammatory mediators in colon tissues

Colon tissues were homogenized in 10 mM PBS (pH 7.2~7.4) containing a protease inhibitor cocktail (Sigma-Aldrich, U.S.A.). Thus obtained suspensions were centrifuged at 2, 000*g* for 15 min at 4°C. The supernatant was collected for detecting the level of H_2O_2. The MPO activity was quantified by an ELISA kit.

Quantification of neutrophils in colonic tissues

Counts of neutrophils in colonic tissues were analyzed by flow cytometry. In brief, colon tissues were incubated in HBSS containing 1 mg/ml collagenase D (Roche Diagnostics, Germany) and 5 μg/ml DNase I (Sigma-Aldrich, U.S.A.) at 37°C for 20 min with gentle agitation, and then filtered passed through a 70-μm cell strainer. Subsequently, single cell suspensions were incubated with anti-CD11b antibody and anti-Ly-6G antibody, and subjected to flow cytometry analyses.

Quantification of the retention of CLP and luminol in the colon after enema administration

Colitis in C57BL/6 mice was induced according to the above mentioned procedures. The diseased mice were randomly assigned into two groups, which were separately received 0.1 ml of saline containing 50 mg/ml CLP nanoparticles or luminol at the same dose of the luminol unit via enema administration after they were anesthetized with isoflurane. At predefined time points, mice were euthanized and colonic tissues were isolated. Both CLP and luminol contents were quantified by high-performance liquid chromatography (HPLC, Prominence-i LC-2030C, Shimadzu) after the colons were homogenized in PBS. For CLP, a Shim-pack GIST C18 column (250 × 4.6 mm, particle size = 5 μm) and a RF-20A fluorescence detector were employed. The excitation wavelength was set at 401 nm, while the emission wavelength was at 660 nm. The mobile phase consisted of water and methanol at a volume ratio of 10:90, with a flow rate of 1.0 ml/min. The column temperature was 40°C. In the case of luminol, it was detected at 240 nm. The mobile phase was consisted of aqueous solution containing 25 mM ammonium acetate and acetonitrile, with a linear gradient elution: 0-30 min, 5-55% acetonitrile. Other conditions were similar to those used for CLP quantification. Also, in vivo fluorescence imaging was performed for mice administered with CLP nanoparticles.

Analyses of neutrophils, MPO, and H_2O_2 in tumor tissues

To establish A549 xenografts in BALB/c nude mice, A549 cells (1×10^7 cells) were subcutaneously inoculated into the left armpit of each mouse. When the tumor volume reached ~1,500 mm^3, mice were euthanized. Tumors were collected and homogenized in PBS. After centrifugation at 1, 6000*g* for 10 min at 4°C, the levels of MPO and H_2O_2 in the supernatant were detected using a MPO ELISA kit and an Amplex red hydrogen peroxide/peroxidase assay kit, respectively. Additionally, tumor tissues were fixed with formalin, and immunofluorescence analyses of neutrophils and MPO were performed on paraffin sections. After the

nuclei were stained with DAPI, fluorescence images were acquired by CLSM.

Histological assessment

Histological sections were scored as the summation of the epithelium and the infiltration. The standards are as follows for the epithelium (E): 0, normal morphology; 1, loss of goblet cells; 2, loss of goblet cells in large areas; 3, loss of crypts; and 4, loss of crypts in large areas. For the infiltration (I), it was evaluated by the following standard scores: 0, no infiltrate; 1, infiltrate around the crypt basis; 2, infiltrate reaching the muscularis mucosae; 3, extensive infiltration reaching the muscularis mucosae and thickening of the mucosa with abundant edema; and 4, infiltration of the submucosa. The total histological scores were presented as E + I.

In vivo safety tests in mice

Preliminary in vivo safety studies were performed in male Kunming mice. To this end, mice (6 weeks old, 23-27 g) were randomly assigned into three groups ($n = 6$). The control group was i.v. administered with saline, while the other two groups were treated with a single dose of CLP nanoparticles at 65 or 130 mg/kg of Ce6 by i.v. injection. At predetermined time intervals post injection, mice were weighed and their behaviors were observed for any signs of illness each day. After 14 days, animals were euthanized. Blood samples were collected for hematological analysis (Sysmex KX-21, Sysmex Co., Japan). Major organs were isolated and weighed. H&E stained histological sections were then prepared.

Supplementary Figures

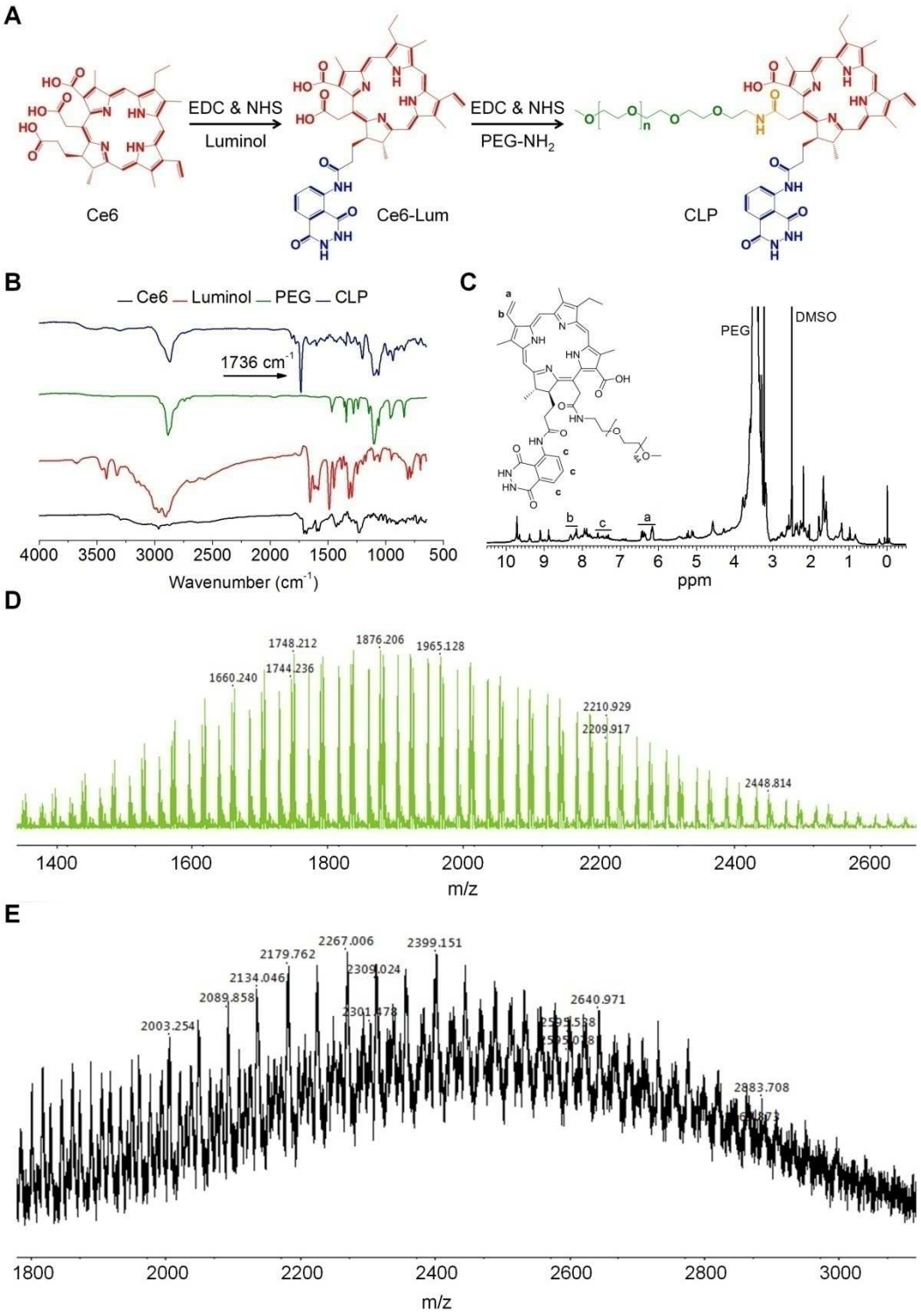

Fig. S1. Synthesis and characterization of a CLP conjugate. (**A**) A synthetic route for the designed CLP conjugate. EDC,1-ethyl-3-(3-dimethylaminopropyl)carbodiimide hydrochloride; NHS, N-hydroxysuccinimide; Ce6-Lum, luminol-Ce6 conjugate. (**B**) FT-IR spectra of Ce6, luminol, PEG, and the CLP conjugate. (**C**) ^{1}H NMR spectrum of the CLP conjugate in deuterated dimethyl sulfoxide (DMSO-D_6). (**D** and **E**) Matrix-assisted laser desorption/ionization time-of-flight (MALDI-TOF) mass spectra of PEG (**D**) or the CLP conjugate (**E**).

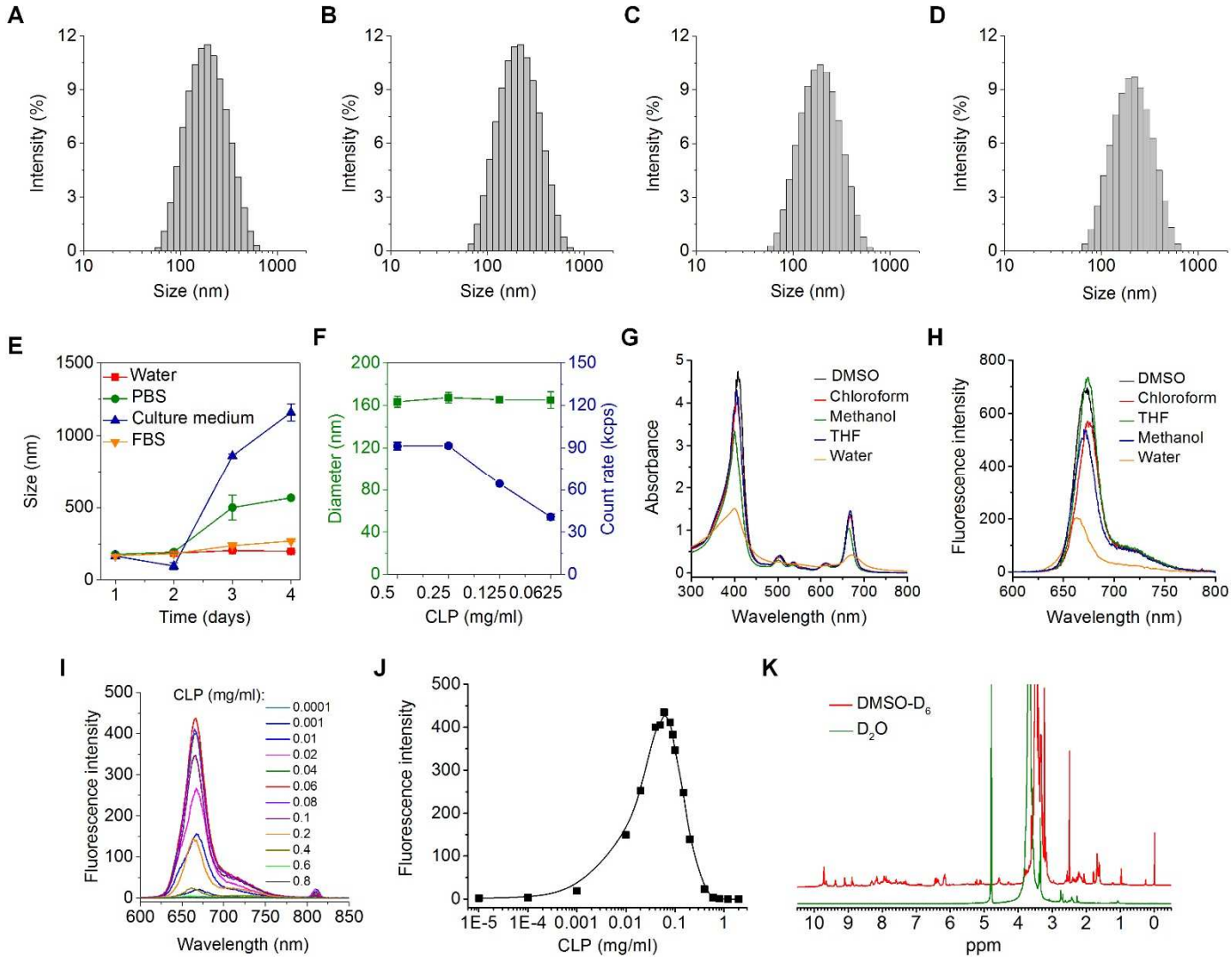

Fig. S2. Characterization of the CLP conjugate and its nanoparticles. (**A** to **D**) Size distribution profiles of CLP nanoparticles in PBS (A), culture medium (B), FBS (C), and serum (D). (**E**) Time-dependent changes in the mean diameter of CLP nanoparticles after incubation in different solutions for varied periods of time. (**F**) Changes in the mean diameter and scattering intensity of CLP nanoparticles upon dilution in deionized water. (**G** and **H**) UV-visible (G) or fluorescence (H) spectra of CLP in different solvents. The concentration of the CLP conjugate was 0.1 mg/ml for both UV-visible and fluorescence spectroscopy. DMSO, dimethyl sulfoxide; THF, tetrahydrofuran. (**I** and **J**) Fluorescence emission spectra of the CLP conjugate (I) and its fluorescence intensities at 665 nm (J) in deionized water at various concentrations. The excitation wavelength was 401 nm. (**K**) ^{1}H NMR spectra of the CLP conjugate in deuterium oxide (D_2O) or DMSO-D_6. In both cases, 20 mg CLP was dissolved in 0.7 ml of D_2O or DMSO-D_6. Data in (E, F) are means ± SEM (n = 3).

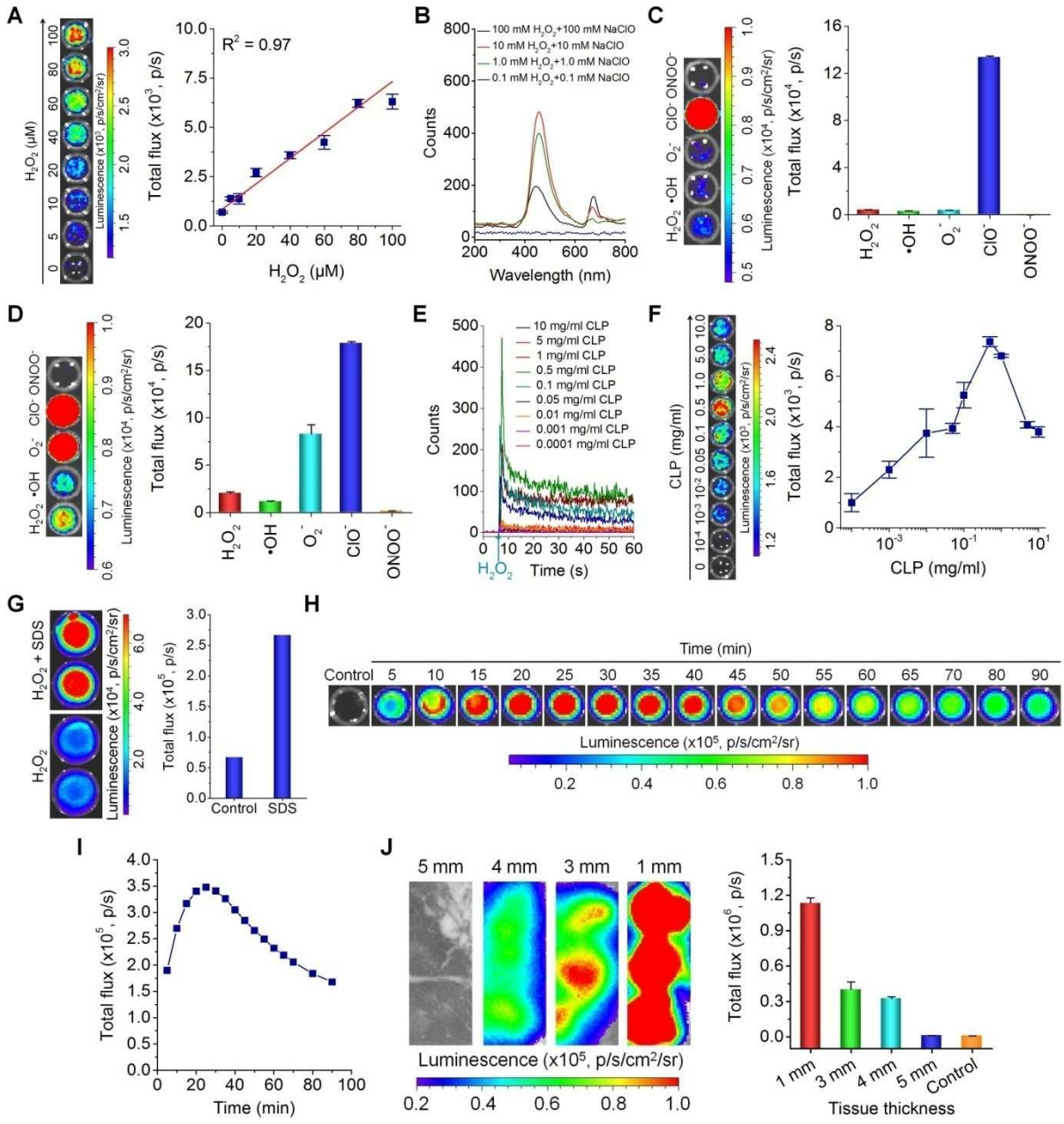

Fig. S3. Luminescence properties of the CLP conjugate under different conditions. (**A**) The effect of H_2O_2 concentration on CLP luminescence at 1 mg/ml. (**B**) Luminescence spectra of the CLP conjugate at 0.1 mg/ml in the presence of different concentrations of H_2O_2 and NaClO. The spectra were acquired with a fiber optic spectrometer. (**C** and **D**) Luminescence of 0.5 mg/ml CLP incubated with different reactive species at 50 μM (C) or 500 μM (D). (**E**) Time-resolved luminescent signals of various concentrations of the CLP conjugate in the presence of 100 mM H_2O_2. (**F**) CLP concentration-dependent luminescence in the presence of 50 μM H_2O_2. (**G**) Luminescent images (left) and quantitative data (right) of the luminescence of the CLP conjugate at 0.3 mg/ml in the presence of 33 mM H_2O_2 with or without the existence of 2.3 mM SDS. (**H** and **I**) Typical luminescent images (H) and quantitative data (I) showing the time-dependent change in luminescent signals of 0.5 mg/ml CLP incubated with 100 mM H_2O_2. (**J**) Penetration of the CLP luminescence through porcine muscle tissues with varied thickness. The luminescent images of CLP at 1.0 mg/ml were acquired in the presence of 100 μM H_2O_2, 30 mU MPO, and 100 mM Cl^-, after the black plate was covered with muscle tissues with varied thickness. For quantification of the luminescent signals by an IVIS Spectrum imaging system, the parameters were set as follows: exposure = 5 min, f/stop = 1, binning = 8, FOV = 6.6 or 12.8 cm. Data in (A, C, D, F, J) are means ± SEM (n = 3).

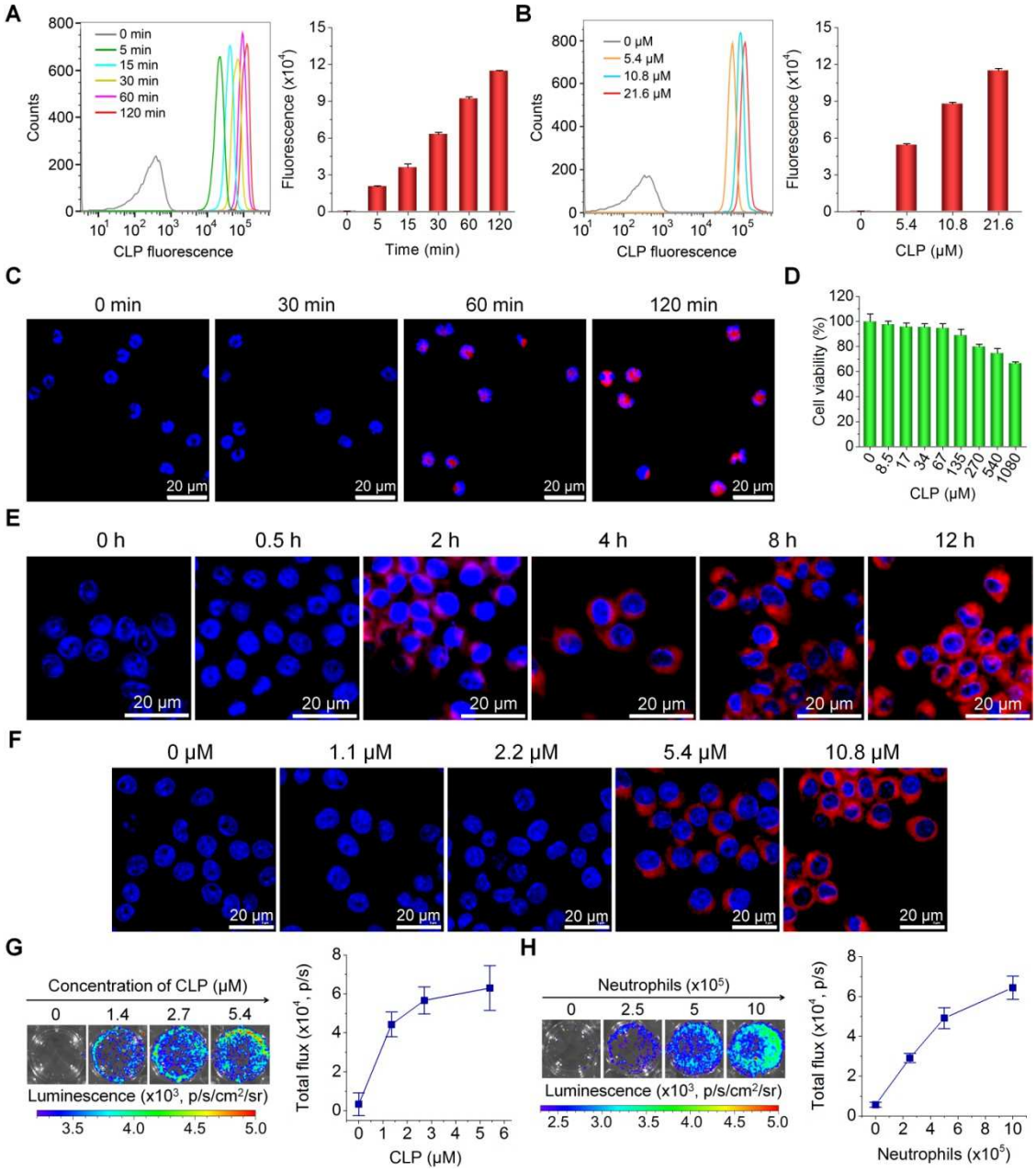

Fig. S4. Intracellular uptake of CLP nanoparticles and in vitro luminescence imaging in neutrophils. (**A** and **B**) Quantification of time-dependent (A) or dose-response (B) cellular internalization of CLP nanoparticles by neutrophils isolated from the peritoneal exudate cells of mice pre-stimulated with thioglycollate. The dose of CLP nanoparticles was 100 μg/ml (21.6 μM) to examine the time effect, while the dose-response effect was tested after 2 h of incubation. The left panels show representative flow cytometric curves, while the right histograms indicate quantitative data. (**C**) Confocal microscopy images of time-dependent uptake of 100 μg/ml (21.6 μM) CLP nanoparticles in neutrophils. Nuclei were stained with DAPI. (**D**) Cell viability of neutrophils after incubation with different doses of CLP nanoparticles for 2 h. (**E** and **F**) Fluorescence images illustrating time (E) and dose (F) dependent cellular uptake of CLP nanoparticles in RAW264.7 macrophages. For time-dependent experiments, the dose of CLP nanoparticles was 50 μg/ml (10.8 μM), while macrophages were incubated with various doses of CLP nanoparticles for 8 h to examine the dose-response internalization. (**G** and **H**) Luminescent signals in neutrophils as a function of the CLP dose (G) or neutrophil count (H). In both cases, neutrophils were stimulated with 100 ng/ml PMA for 1 h, followed by the addition of predetermined doses of CLP. Data in (A, B, D to F) are means ± SEM (A, B, G, H, $n = 3$; D, $n = 4$).

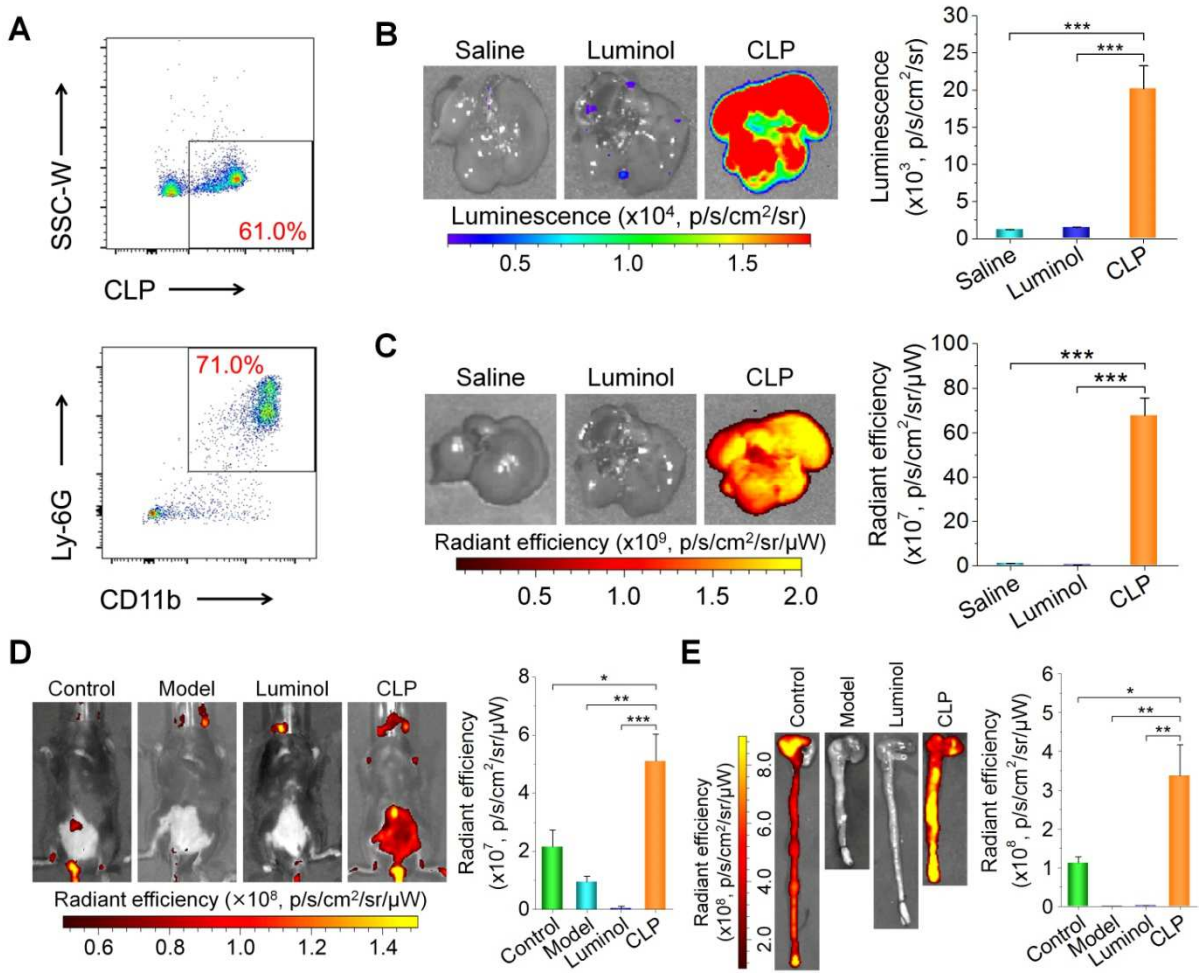

Fig. S5. In vivo imaging in different mouse models of inflammation. (**A**) Flow cytometric analysis of the cellular distribution of CLP nanoparticles in peritoneal neutrophils ($CD11b^{+}Ly\text{-}6G^{+}$) from mice with peritonitis. At 0.5 h after i.p. administration of CLP nanoparticles in peritonitis mice, the animals were euthanized, and their peritoneal exudate cells were collected for cell sorting analysis. (**B**) Ex vivo luminescence imaging (left) and quantification of luminescent intensities (right) of isolated hepatic tissues from mice with acetaminophen (APAP)-induced acute liver injury. (**C**) Ex vivo fluorescence images (left) and quantitative data (right) indicating the accumulation of CLP nanoparticles in the liver. In both cases, after 24 h of challenging via i.p. injection of APAP at 300 mg/kg, mice in the saline group were i.v. injected with saline, while mice in the luminol and CLP groups were i.v. administered with free luminol or CLP nanoparticles (5 mg in each animal) at the same dose of the luminol unit, respectively. The liver was excised immediately for ex vivo imaging after in vivo imaging. For fluorescence imaging, the excitation wavelength was 430 nm, with emission at 680 nm. (**D** and **E**) In vivo (D) and ex vivo (E) fluorescence imaging of animals or tissues. The control group represents healthy mice treated with CLP nanoparticles, while the model group denotes diseased mice administered with saline. In the luminol and CLP groups, mice with colitis were treated with free luminol and CLP nanoparticles (5 mg per mouse) at the same dose of the luminol unit, respectively. At 15 min after different treatments via enema, in vivo fluorescence images were acquired. Then, the mice were euthanized, and their colonic tissues were excised for ex vivo imaging. In both cases, the excitation wavelength for was 430 nm, with emission at 680 nm. Data are means ± SEM (B, C, $n = 4$; D, E, $n = 5$). $^{*}P < 0.05$; $^{**}P < 0.01$; $^{***}P < 0.001$.

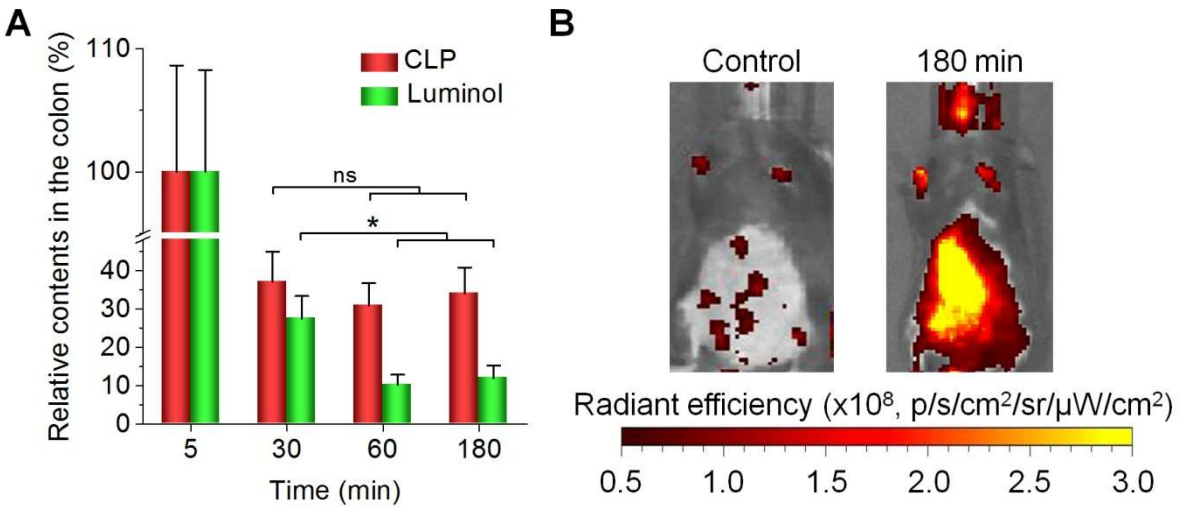

Fig. S6. The retention of CLP and luminol in the colon after enema administration in colitis mice. (**A**) The relative contents of CLP and luminol in colonic tissues isolated from mice with DSS-induced colitis. Quantification was performed by HPLC at various time points after local administration of 5 mg CLP nanoparticles or free luminol at the same dose of the luminol unit in each animal. (**B**) Representative in vivo fluorescence images indicate the presence of CLP at 180 min after enema administration. Data are means ± SEM ($n = 4$). ns, no significance; *$P < 0.05$.

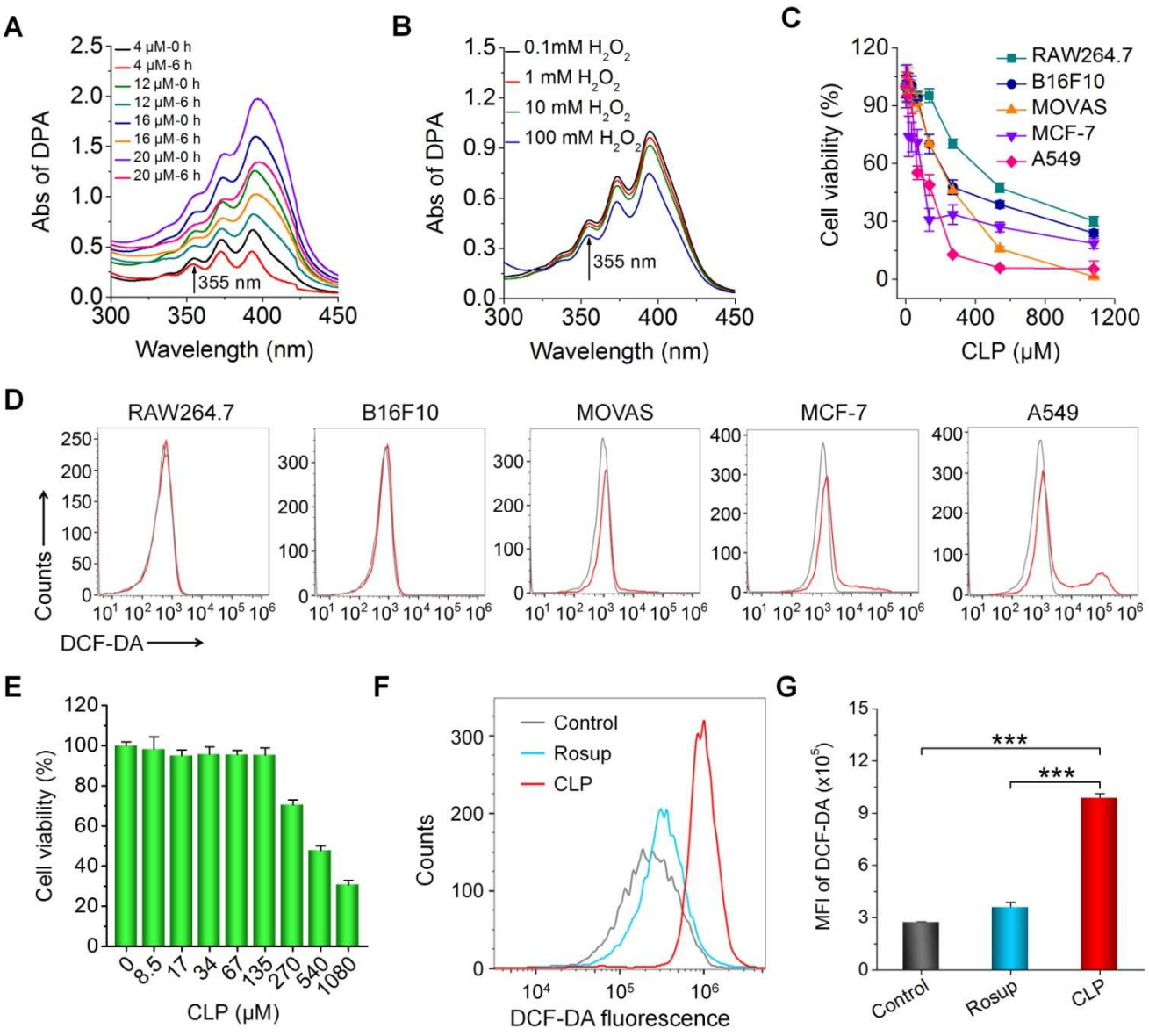

Fig. S7. In vitro antitumor activity of CLP nanoparticles. (**A** and **B**) The effects of CLP dose (A) and H_2O_2 concentration (B) on the generation of $^1O_2$, as quantified using DPA as a probe. The images show UV absorbance spectra of DPA. For the dose effect, quantification was performed after CLP nanoparticles were incubated with 100 mM H_2O_2 for 6 h. To examine the influence of the H_2O_2 concentration, absorbance was measured after 6 h of incubation with 20 μM CLP nanoparticles. (**C**) Cell viability values of different cells (including RAW264.7 murine macrophages, B16F10 mouse melanoma cells, MOVAS mouse aortic vascular smooth muscle cells, MCF-7 human breast cancer cells, and A549 cells) after incubation with various doses of CLP nanoparticles for 24 h. (**D**) Representative flow cytometric curves show intracellular ROS levels in different cell lines using a fluorescent probe DCF-DA. The gray curves represent control cells treated without DCF-DA, while the red curves are from DCF-DA-probed cells. The corresponding quantitative data are shown in **Fig. 5E**. (**E**) Cytotoxicity of various doses of CLP nanoparticles in RAW264.7 murine macrophages after 24 h of incubation. (**F** and **G**) Representative cytometric profiles (F) and quantified data (G) indicating the relative intracellular ROS levels in A549 cells after different treatments. Cells in the control group were treated with culture medium alone, while the CLP group was incubated with CLP nanoparticles at 200 μg/ml (43.2 μM) for 4 h. The positive control group was treated with Rosup. Data are means ± SEM (C, E, $n = 4$; G, $n = 3$). ***$P < 0.001$.

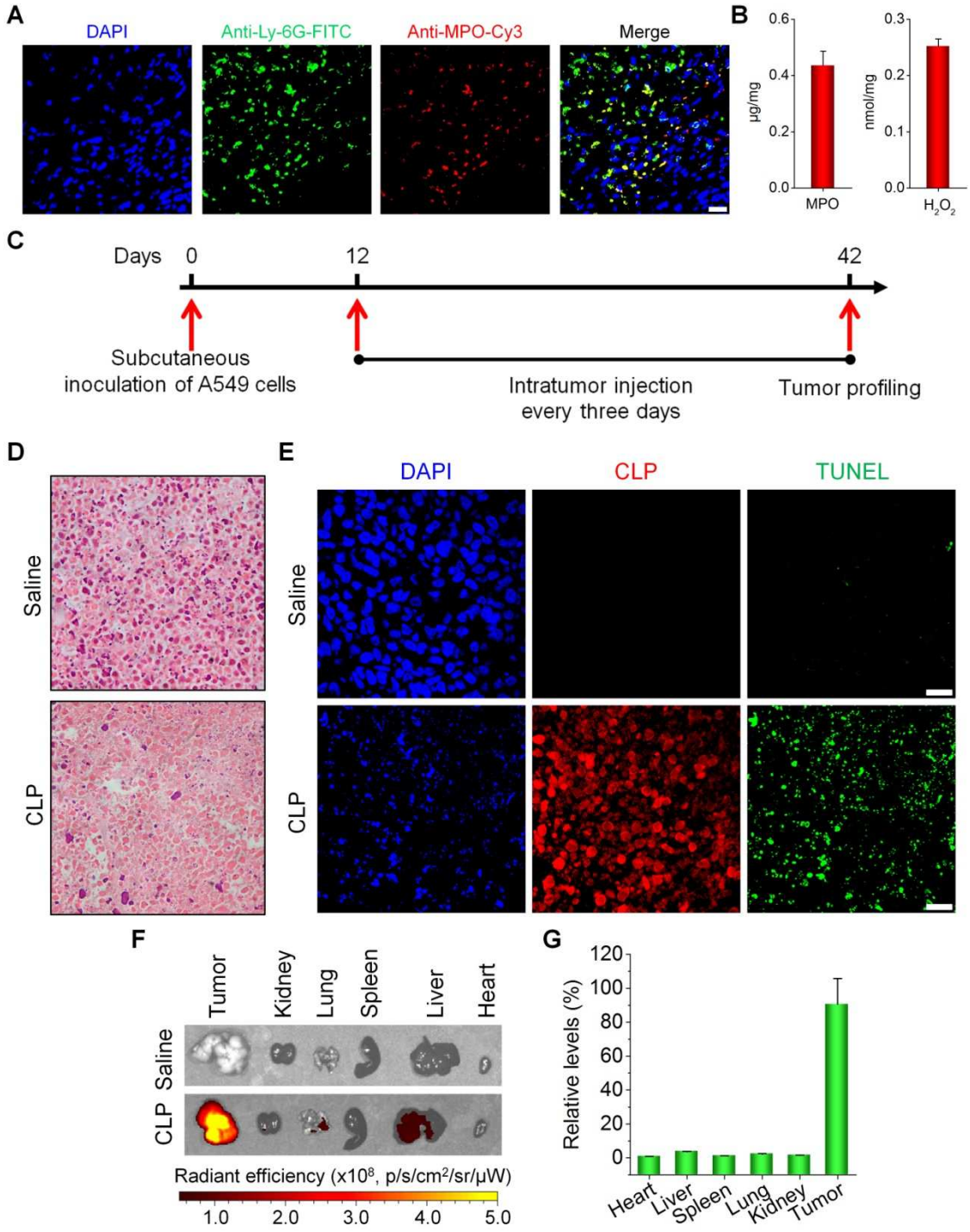

Fig. S8. Tumor therapy after intratumoral administration of CLP nanoparticles in mice bearing A549 xenografts. (**A**) Immunofluorescence images showing neutrophils and MPO in tumors. (**B**) Quantified MPO and H_2O_2 levels in tumor tissues. A549 cells were inoculated subcutaneously into nude mice to establish xenografts. Tumors were excised for analyses when their volume reached ~1500 mm^3. (**C**) The treatment regimen for tumor therapy by intratumoral injection of CLP nanoparticles. (**D**) H&E-stained tumor sections after treatment via intratumoral injection of saline or CLP nanoparticles. (**E**) Confocal microscopy analysis of the distribution of CLP nanoparticles and cell apoptosis in tumor sections after 30 days of treatment via intratumoral injection of CLP nanoparticles at 3.25 mg/kg of Ce6. (**F** and **G**) Ex vivo images (F) and quantification (G) of the CLP distribution in different tissues after intratumoral administration of CLP nanoparticles containing 3.25 mg/kg of Ce6. Mice in the saline group were treated with saline. Scale bars, 20 μm. Data in (B, G) are means ± SEM (B, $n = 4$; G, $n = 6$).

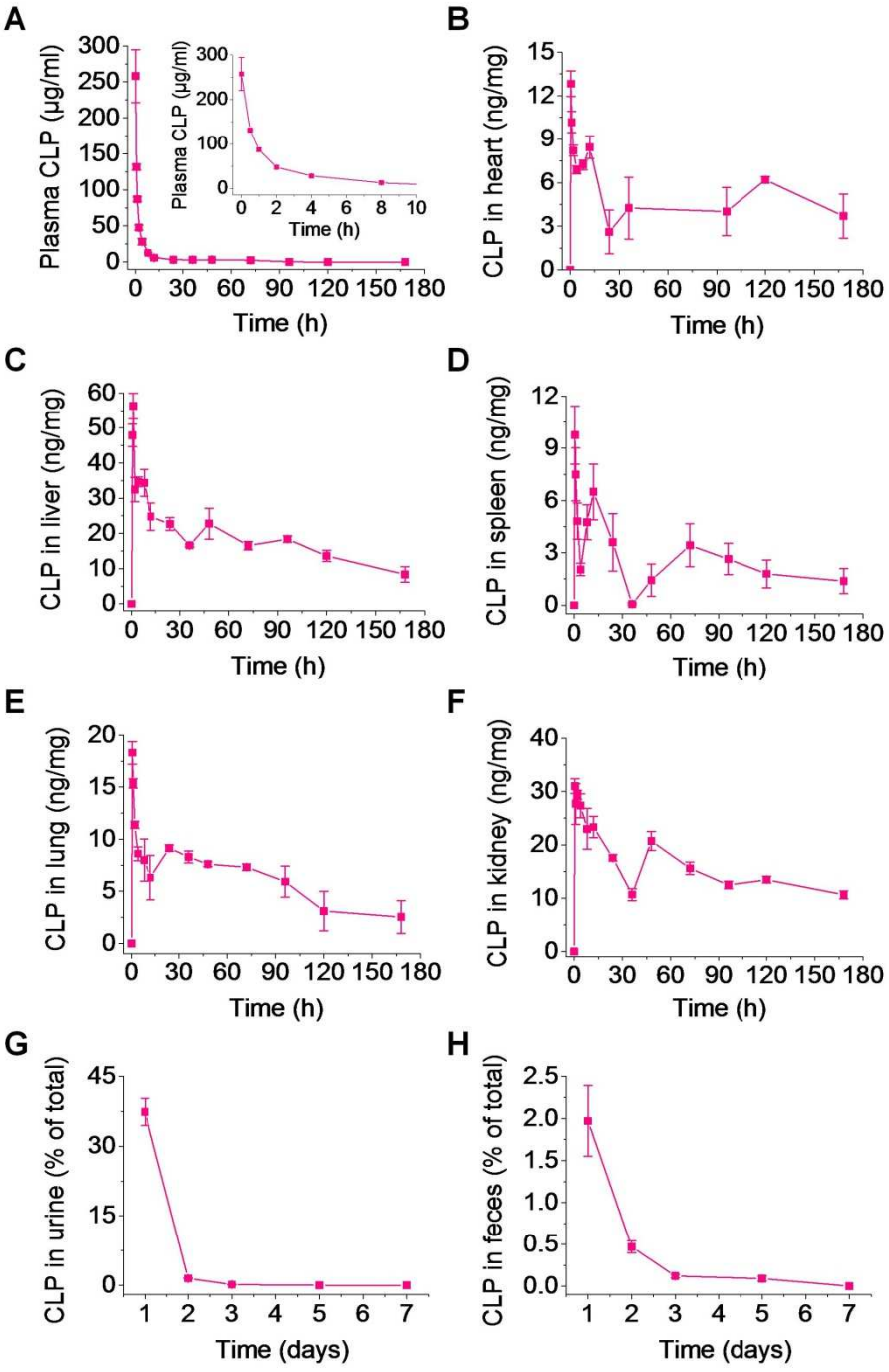

Fig. S9. In vivo pharmacokinetic, tissue distribution, and elimination profiles of CLP after intravenous administration. (**A**) The plasma CLP concentration-time curve after intravenous injection of CLP nanoparticles at 25 mg/kg. (**B** to **F**) CLP levels in heart (B), liver (C), spleen (D), lung (E), and kidney (F) at defined time points. (**G** and **H**) Elimination of CLP through urine (G) and feces (H) at different time points after i.v. administration of CLP nanoparticles at 25 mg/kg. In all cases, CLP concentrations were quantified by HPLC. Data are means ± SEM (A to F, $n = 5$; G and H, $n = 6$).

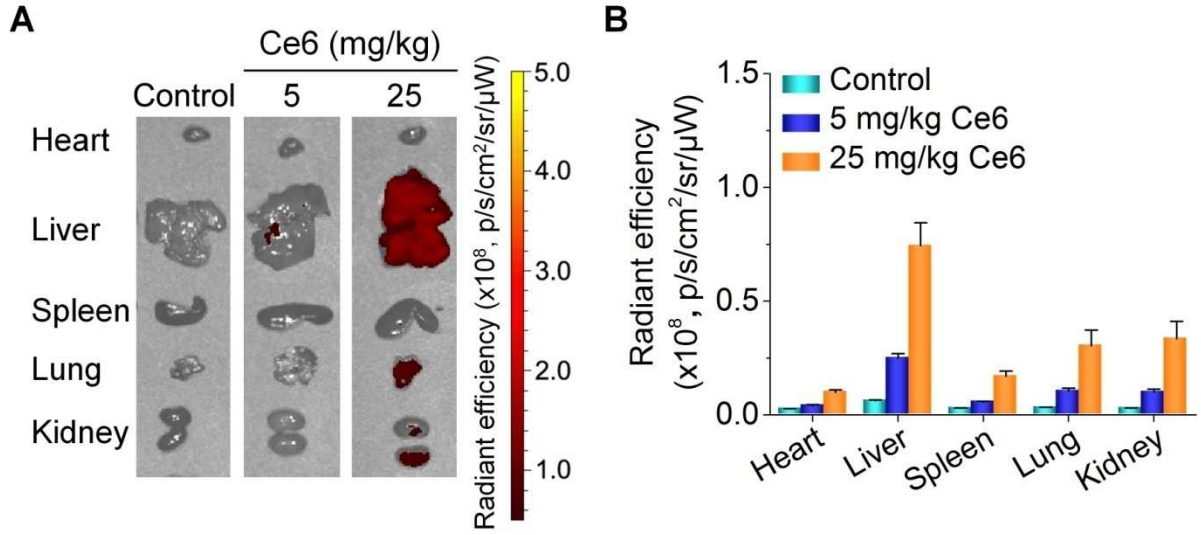

Fig. S10. Tissue distribution of CLP nanoparticles after intravenous administration in mice bearing A549 xenografts. (**A** and **B**) Ex vivo fluorescence images (A) and quantification (B) of the tissue distribution of intravenously administered with CLP nanoparticles at 5 or 25 mg/kg of Ce6. Mice in the control group were treated with saline. At day 7 after the last administration, different organs were isolated for ex vivo imaging. Data are means ± SEM (n = 4).

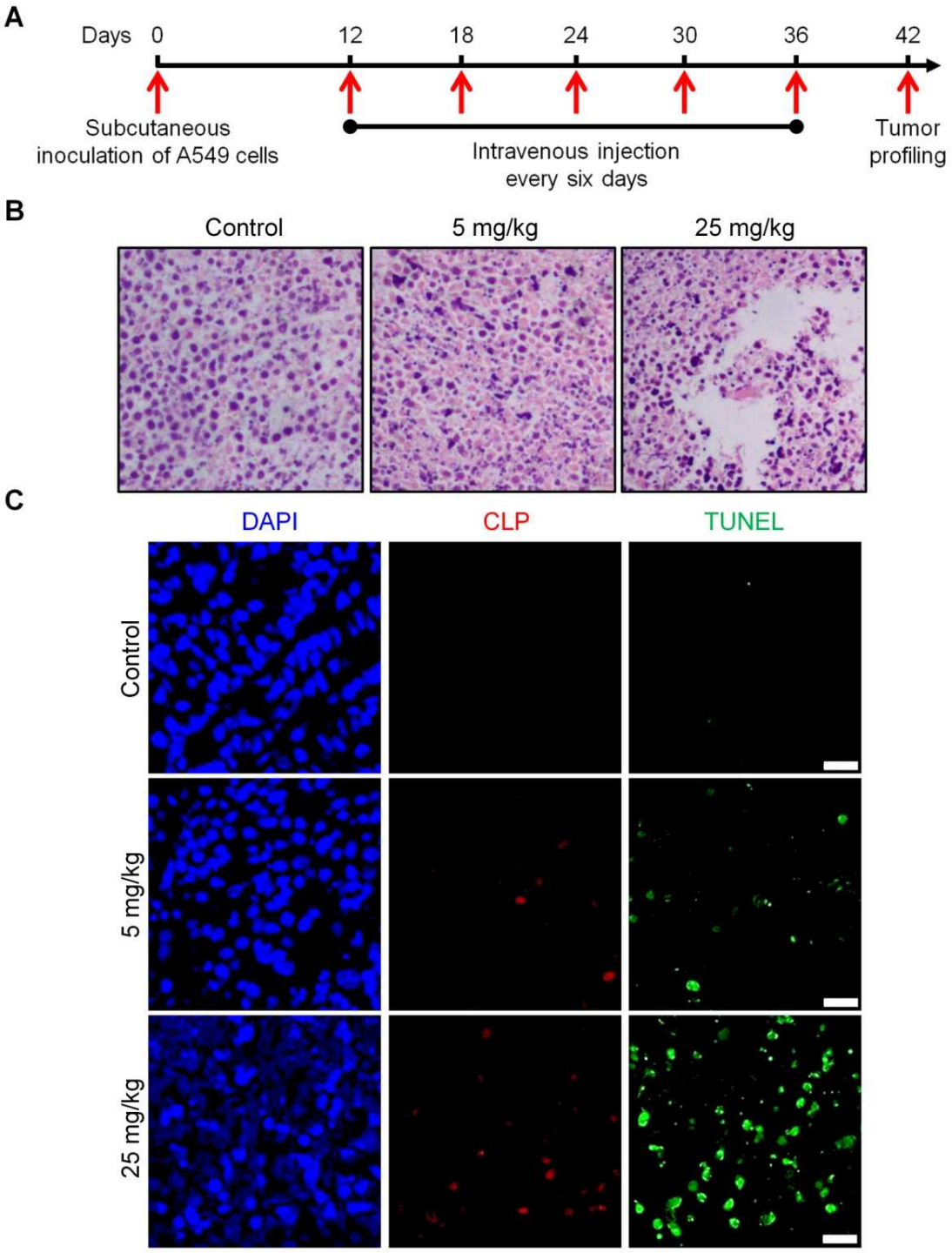

Fig. S11. Tumor therapy after intravenous administration of CLP nanoparticles in mice bearing A549 xenografts. (**A**) The experimental protocols for tumor therapy by i.v. injection of CLP nanoparticles. (**B**) H&E-stained histological sections after 30 days of treatment with saline or CLP nanoparticles. (**C**) Confocal microscopy observation of the CLP distribution and TUNEL assay of cell apoptosis in tumor sections. Mice in the control group were treated with saline. Tumor tissues were excised at day 30 after different treatments. Scale bars, 20 μm.

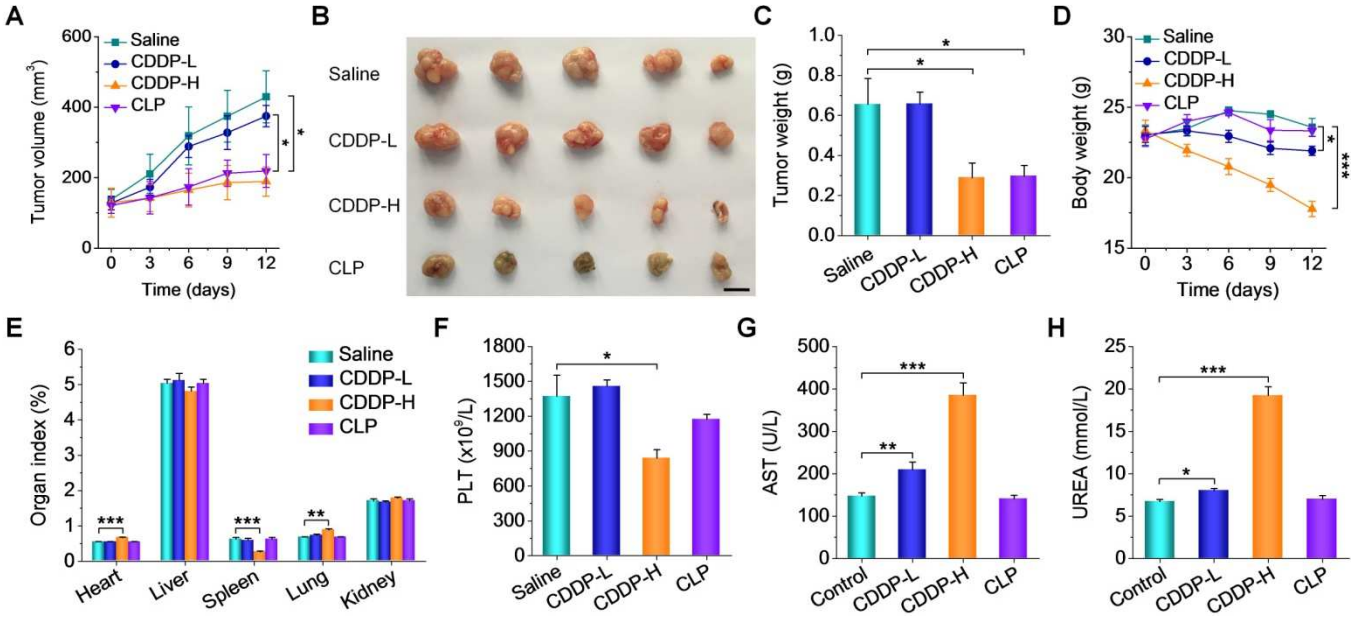

Fig. S12. Comparison of in vivo efficacy and safety of CLP nanoparticles with CDDP. (**A**) Changes in the tumor volume of A549 xenografts during different treatments. (**B** and **C**) Digital photos (B) and quantified tumor weight (C) of excised tumors at day 14 after treatment. Scale bar, 1 cm. (**D**) Changes in the body weight of A549 xenograft-bearing mice. (**E**) The organ index values of representative organs from mice at day 14. (**F**) The levels of platelet (PLT). (**G** and **H**) The plasma levels of aspartate aminotransferase (AST) (G) and urea (UREA) (H). After A549 xenografts were established in mice, the CLP group was treated with CLP nanoparticles at a dose equivalent to 25 mg/kg of Ce6. Mice in the CDDP-L and CDDP-H groups were administered with CDDP at 1 and 6 mg/kg CDDP, respectively. The control group was injected with saline. All treatments were performed by i.v. administration once every three days. Data are means ± SEM (n = 5). *P < 0.05; **P < 0.01; ***P < 0.001.

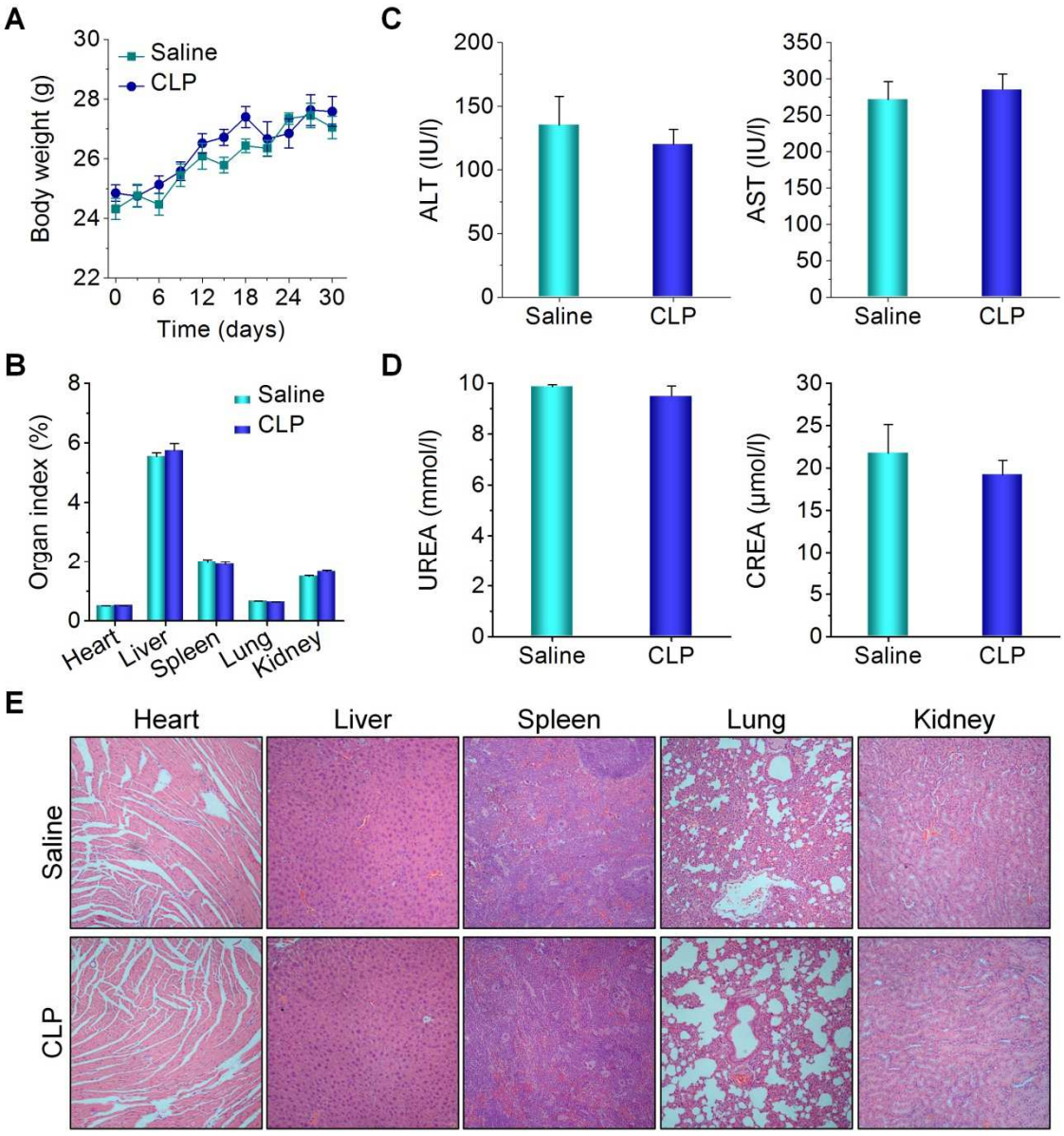

Fig. S13. Safety study after intratumoral administration of CLP nanoparticles in A549 xenograft–bearing mice. (**A**) Changes in body weight of mice during intratumoral administration of CLP nanoparticles at 3.25 mg/kg of Ce6 every three days for 30 days. (**B**) The organ index values of major organs after treatment with CLP nanoparticles for 30 days. (**C**) Plasma levels of alanine aminotransferase (ALT) and aspartate aminotransferase (AST) after treatment with CLP nanoparticles. (**D**) Levels of blood urea (UREA) and creatinine (CREA). The plasma levels of ALT and AST are closely related to hepatic functions, while UREA and CREA levels are associated with renal functions. When the levels of these biomarkers are above the normal ranges, they indicate significant hepatic and renal injuries. (**E**) H&E-stained histological sections of major organs. In all cases, blood samples and different tissues were collected for analyses at day 30 after treatment with saline or CLP nanoparticles. Mice in the saline group were treated with saline. Data are means ± SEM (n = 6).

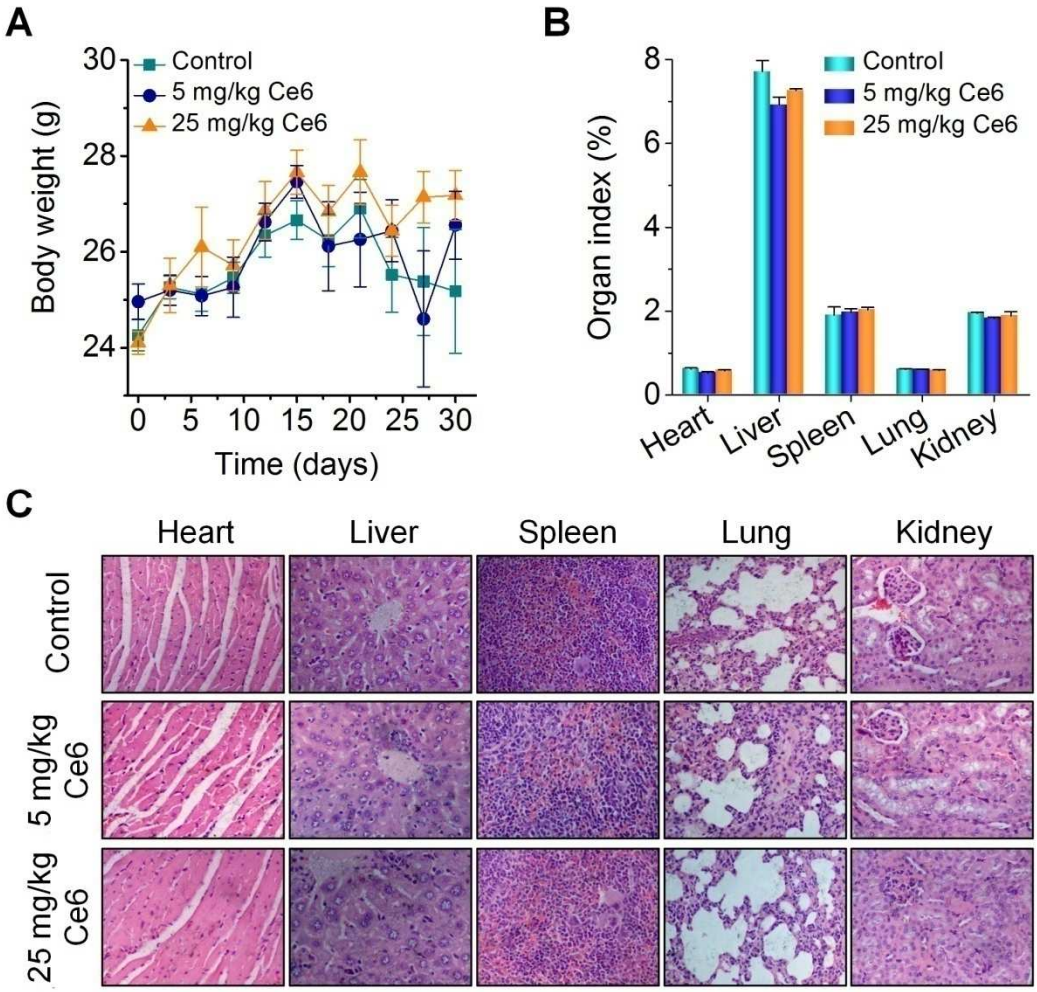

Fig. S14. Safety profiles of CLP nanoparticles in A549 xenograft–bearing mice during and after 30 days of intravenous injection. (**A**) Changes in body weight during 30 days of treatment with CLP nanoparticles at 5 or 25 mg/kg of Ce6 every 6 days. (**B**) Organ index of major organs at day 30 after treatment with intravenously administered with CLP nanoparticles. (**C**) H&E-stained histological sections of major organs after different treatments. Mice in the control group were treated with saline. Data are means ± SEM (n = 4).

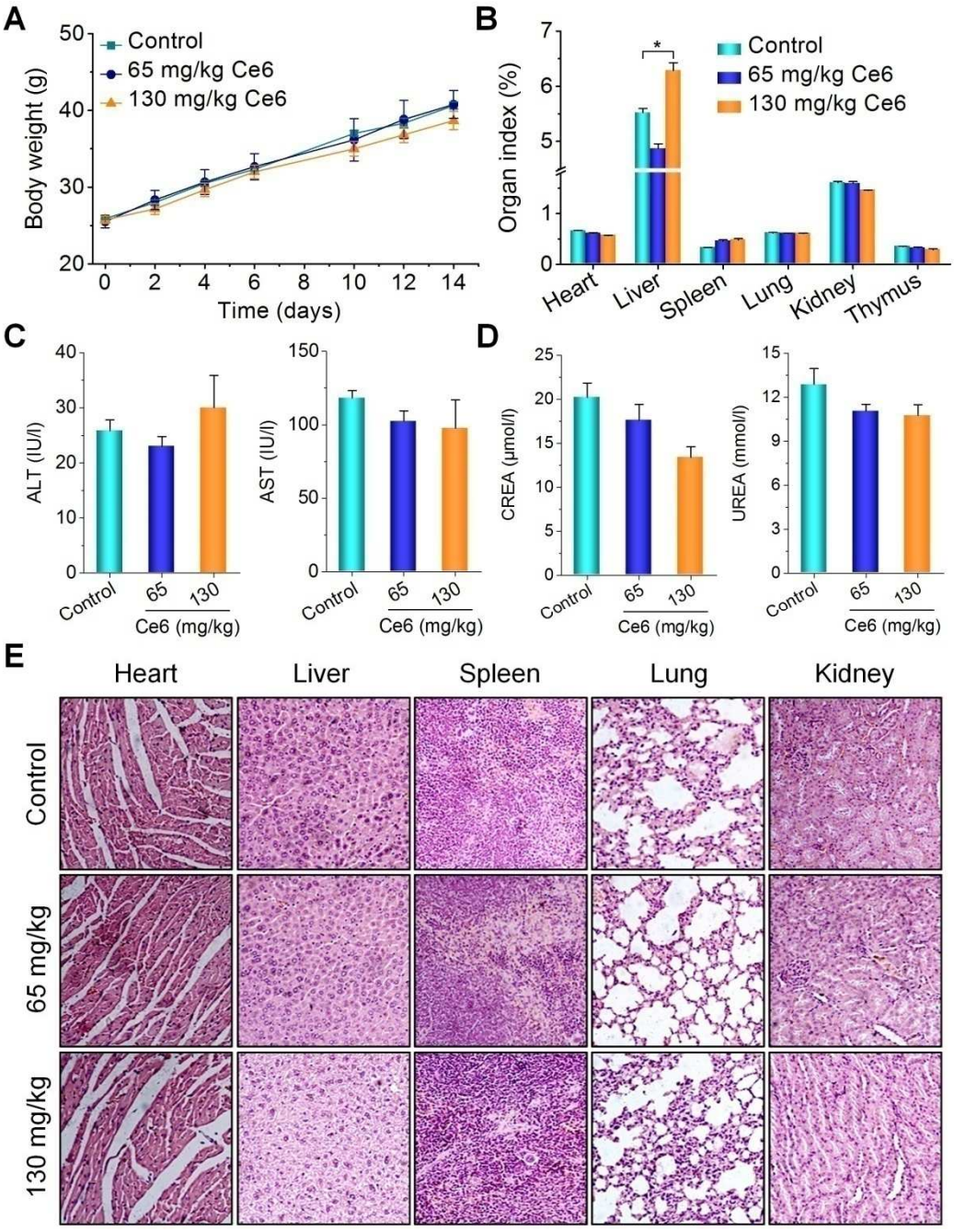

Fig. S15. Acute toxicity evaluation of CLP nanoparticles after a single intravenous injection in healthy mice. (**A**) Body weight changes of mice after intravenous injection of CLP nanoparticles at 65 or 130 mg/kg of Ce6. Mice in the control group were treated with saline. Mice were monitored immediately after i.v. administration of CLP nanoparticles. (**B**) The organ index values of major organs at day 14 after treatment with saline or CLP nanoparticles. (**C** and **D**) Plasma levels of ALT and AST (C) as well as UREA and CREA (D) after different treatments. (**E**) H&E-stained histological sections of major organs isolated from mice at day 14 after different treatments. Data are means ± SEM ($n = 6$). *$P < 0.05$.

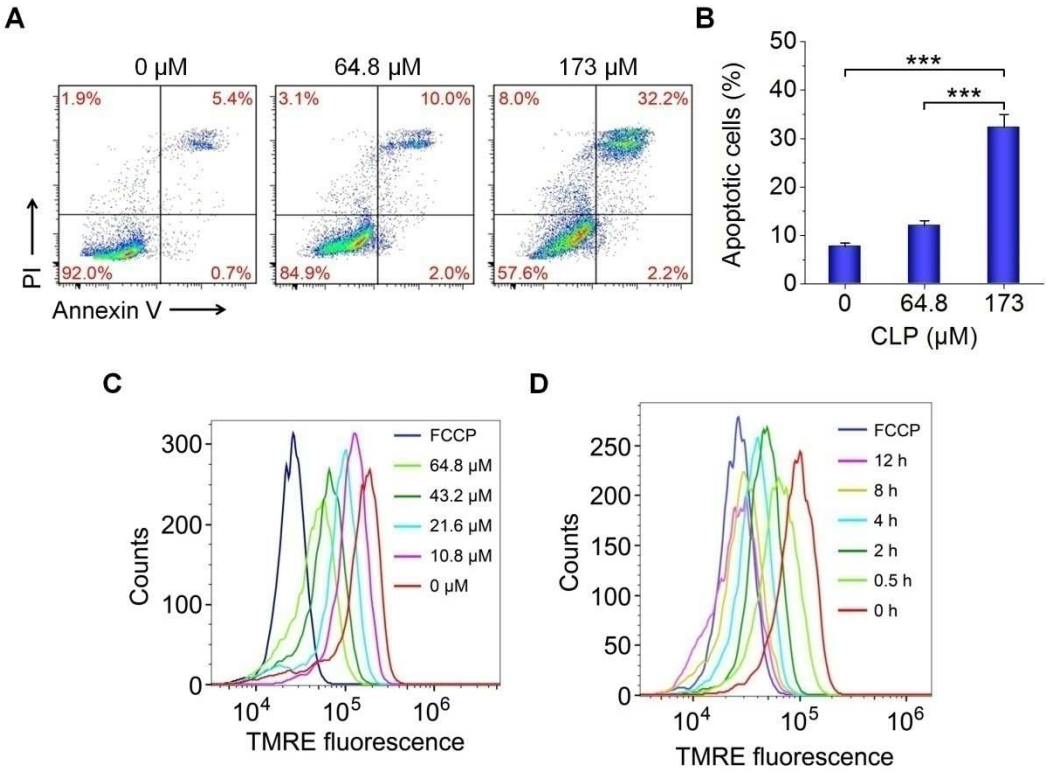

Fig. S16. Mechanistic studies of in vitro antitumor activity of CLP nanoparticles in A549 cells. (**A** and **B**) Representative flow cytometric profiles (A) and quantitative analysis (B) of cell apoptosis after 24 h of incubation with various doses of CLP. (**C** and **D**) Flow cytometric analysis of mitochondrial membrane potential of A549 cells after different treatments. Representative flow cytometric profiles of A549 cells after 12 h of incubation with varied doses of CLP nanoparticles (C) or incubation with 64.8 μM CLP nanoparticles for different periods of time (D). The corresponding quantitative data are shown in Fig. 6, B and C. In both cases, FCCP was used as a positive control that can effectively depolarize mitochondrial membrane potential. Data in (B) are means ± SEM (n = 4). ***P < 0.001.